Dynamics of Polyethersulfone Phenylene Rings: A Quasielastic Neutron Scattering Study

I. Quintana,[†] A. Arbe,[*,‡] J. Colmenero,[†,‡,§] and B. Frick[||]

Departamento de Física de Materiales UPV/EHU, Apartado 1072, 20080 San Sebastián, Spain, Unidad Física de Materiales (CSIC−UPV/EHU), Apartado 1072, 20080 San Sebastián, Spain, Donostia International Physics Center, Apartado 1072, 20080 San Sebastián, Spain, and Institut Laue-Langevin, BP 156, 38042 Grenoble Cedex 9, France

Received November 30, 2004; Revised Manuscript Received February 18, 2005

ABSTRACT: By means of quasielastic neutron scattering, we have studied the hydrogen dynamics in glassy polyethersulfone, revealing the phenylene ring motions. The combination of a time-of-flight (TOF) and a backscattering spectrometer has allowed us to cover the microscopic and mesoscopic time scales ($\sim 10^{-13}-10^{-9}$ s) in a momentum transfer region well-suited to characterize local motions ($\sim$0.4...2 Å^{-1}). After a first step reflecting the fast processes undergone by the hydrogen below $\sim$2 ps, the decay of the intermediate scattering function can be described by the occurrence of a combined motion of the phenylene ring. This consists of π-flips and an additional process, faster and more restricted in space. We have interpreted this last motion as oscillations of increasing amplitude with temperature, which would emerge from the fluctuation of the local phenyl ring environment. Because of the structural disorder, both motions, π-flips and oscillations, show broadly distributed characteristic times, extending over several orders of magnitude. The coincidence of the activation energies for π-flips and γ-relaxation on one hand and for oscillations and δ-relaxation on the other hand confirms their respective strong correlation. Discrepancies in the absolute values of the corresponding characteristic times reflect, however, the higher complexity of the secondary relaxations in these kinds of systems.

1. Introduction

Polymers containing aromatic rings usually present high values for their glass-transition temperature T_g and, at room temperature, offer a wide range of applications including, e.g., gas separation or their use as structural materials (engineering thermoplastics). The mechanically advantageous behavior and other valuable properties of these kinds of polymers relate to microscopic relaxation mechanisms that, despite large efforts, are not yet satisfactorily identified. The understanding of the good application properties of these systems in terms of microscopic features is the key to the future design of novel materials with tailor-made properties and, therefore, of high interest also from a technological point of view.

The microscopic mobility in the temperature range of utilization of engineering thermoplastics (below T_g) is reflected in the secondary relaxations that are usually characterized by means of relaxation techniques such as mechanical spectroscopy (MS) or dielectric spectroscopy (DS). Since these techniques do not reveal spatial information on the dynamics of the system, very little is known about the molecular mechanisms giving rise to these secondary relaxations. However, during the last years, a great deal of effort has been made in this direction involving numerous MS[1−10] and DS[11−15] experiments in a wide variety of thermoplastics, including, e.g., substituted polycarbonates, copolymers, and blends. The results suggest that the so-called γ-relaxation (located at about 273 K at 1 Hz) is due to the cooperative motion of several units and is closely related to phenylene ring motion. Some *p*-phenylene polymers present, in addition to the γ-relaxation, another relaxation (called δ) at even lower temperatures ($\sim$100 K and 1 Hz), which would also be attributable to motions involving phenylene rings.[8] We note that the rotation of one ring itself would not lead to large dielectric and mechanical losses. Therefore, it seems unlikely to be at the origin of the secondary relaxations unless it is cooperatively linked to the motions or is part of the mechanism causing the relaxations and therefore monitoring them, as it has been repeatedly suggested in the literature.[1,5,11,13,15]

For these reasons, a large series of investigations during last years have been devoted to the study of the phenylene rings present in these systems, including dynamical aspects. The techniques employed are mainly NMR and molecular dynamics calculations. From NMR studies on polycarbonates, polyaryls, and epoxy resins, it has been established that phenylene rings undergo π-flips around the C1−C4 axis (see Figure 1), oscillations around the same axis, and some small amplitude main-chain reorientations.[16−25] A correlation between the γ-relaxation and π-flip motions of the rings has been found through the similarity between the corresponding activation energies.[21,22,24] On the other hand, theoretical calculations and molecular dynamics simulations on systems containing phenylene rings qualitatively agree with the type of motions observed experimentally.[26−35] However, the exact mechanism leading to the occurrence of these flips or the role of these motions on the mechanical properties is still unclear. Thus, additional information based on space/time-resolved techniques is imperative to shed more light on this long-standing problem. Neutron scattering (NS) offers such resolution at a microscopic level.

Author to whom correspondence should be addressed. E-mail: waparmea@sc.ehu.es.
[†] Departamento de Física de Materiales UPV/EHU.
[‡] Unidad Física de Materiales (CSIC−UPV/EHU).
[§] Donostia International Physics Center.
[||] Institut Laue-Langevin.

10.1021/ma047535n CCC: $30.25
Published on Web 03/26/2005

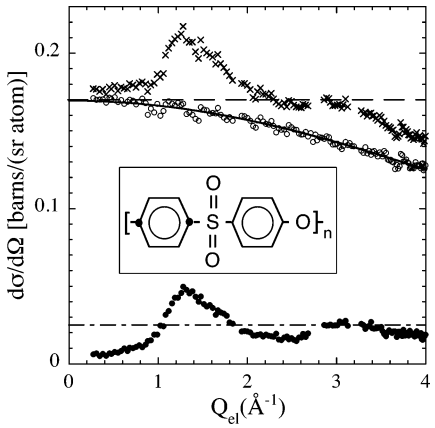

Figure 1. Differential neutron scattering cross sections obtained from D7 measurements for fully protonated PES at 100 K. The full circles correspond to coherent scattering, the empty circles to incoherent scattering, and the crosses to the total scattering. The solid line is a *DWF*-like description of the incoherent data. The dashed (dashed−dotted) line represents the value of $\sigma_{inc}/(4\pi)$ [$\sigma_{coh}/(4\pi)$]. The insert shows the chemical structure of PES, where the C1 and C4 atoms of one phenylene ring have been marked with spots.

With these ideas in mind, we have started to approach this problem applying NS techniques to the investigation of phenylene ring dynamics in different engineering thermoplastics. The first study concerned bisphenol A-polysulfone (BPA-PSF),[36−38] for which the spatial resolution of NS has allowed identification of two kinds of motions of phenylene rings: π-flips and small angle oscillations of increasing amplitude with temperature. The flips could be related to the γ-relaxation, while the oscillations showed a mean activation energy close to that determined for methyl group rotations by NMR and the δ-relaxation by MS. In that study, both motions were considered statistically independent processes and the four rings dynamically equivalent. Some preliminary NS results on bisphenol A-polycarbonate (BPA-PC) and phenoxy (PH) have also been published by now.[39−41]

Within this framework, we present here a thorough NS study on polyethersulfone (PES), a well-known polymer for its application as a membrane for gas separation. Its chemical composition is shown in the insert of Figure 1. Our NS measurements reveal the aromatic hydrogen dynamics, thus reflecting directly the phenylene ring motions. We will show that a phenomenological inspection of the spectral features points to a similar scenario for phenylene ring dynamics to that found in the case of BPA-PSF; consequently, PES data are analyzed by using the same model proposed for that polymer. The obtained microscopic information will be compared to the data available in the literature concerning secondary relaxations in this polymer, trying to contribute to the understanding of the molecular motions behind its good properties. On the other hand, it is noteworthy that the BPA-PSF monomer consists of the same group contained in PES but linked to an isopropylidene group. Therefore, with this study, we will have in addition the opportunity to check the validity of the scenario proposed for BPA-PSF phenylene ring dynamics by answering the question: do diphenylsulfone rings move in a similar way to that globally observed for *all* rings in BPA-PSF?

The NS measurements presented here are the result of a combination of two different spectrometers to cover the microscopic and mesoscopic time scales (~0.1 ps to 1 ns) and a wide momentum transfer (Q) range ($0.4 \leq Q \leq 2$ Å^{-1}). These experiments have allowed us to unveil the phenylene ring dynamics in the polymer membrane under study, PES. A preliminary analysis of the microscopic data can be found in a recent publication.[42] In addition, we show a diffraction measurement with polarization analysis, revealing structural features of PES.

II. Experimental Section

A. Sample. The chemical composition of polyethersulfone, PES, is shown in Figure 1. Molecular weight and polydispersity of the sample supplied by Aldrich Chemical Co. Inc. were $M_n = 16\,900$ g/mol and $M_w/M_n = 1.45$. Differential scanning calorimetry measurements lead to a T_g of 500 K. Samples were vacuum heated near T_g for 24 h prior to the NS experiments. The samples were subjected to the same thermal treatment for the experiments with the different instruments.

B. Neutron Scattering Experiments. Except for neutron spin−echo techniques, the quantity assessed in a neutron scattering (NS) experiment focused on dynamical aspects of the system is the double-differential cross section: the number of scattered neutrons into a solid angle between Ω and $\Omega + d\Omega$, after having exchanged an energy between E and $E + dE$ with the sample, relative to the number of incident neutrons. It has an incoherent and a coherent contribution:

$$\frac{\partial^2\sigma}{\partial\Omega\partial E} = \left(\frac{\partial^2\sigma}{\partial\Omega\partial E}\right)_{inc} + \left(\frac{\partial^2\sigma}{\partial\Omega\partial E}\right)_{coh} \quad (1)$$

The incoherent contribution can be expressed in terms of the incoherent scattering function $S^{\alpha}_{inc}(Q, \omega)$ of the different kinds of nuclei α in the sample weighed by their corresponding incoherent cross sections σ^{α}_{inc} as:

$$\left(\frac{\partial^2\sigma}{\partial\Omega\partial E}\right)_{inc} = \frac{k}{k_o}\sum_{\alpha} N_{\alpha}\frac{\sigma^{\alpha}_{inc}}{4\pi}S^{\alpha}_{inc}(Q, \omega) \quad (2)$$

Here the sum ranges over all the different atomic species (α: H, C, O, S,...) and N_α is the number of nuclei of the α type. $\vec{k}_o$ and $\vec{k}$ are the momenta of the incident and scattered neutrons, Q is the modulus of the momentum transfer $\vec{Q} = \vec{k} - \vec{k}_o$ and $\omega = E/\hbar$. $S^{\alpha}_{inc}(Q, \omega)$ is the Fourier transform of the intermediate incoherent scattering function $S^{\alpha}_{inc}(Q, t)$

$$S^{\alpha}_{inc}(Q, \omega) = \frac{1}{2\pi\hbar}\int S^{\alpha}_{inc}(Q, t)\, e^{-i\omega t}\, dt \quad (3)$$

The double Fourier transform of $S^{\alpha}_{inc}(Q, \omega)$ yields the self-part of the Van Hove correlation function, $G^{\alpha}_{self}(r, t)$, which gives the probability of a given nucleus of the α type to be at distance r from the position where it was located at a time t before. Thus, incoherent scattering looks at correlations between the positions of the same nucleus at different times. The relation between scattering function and Van Hove function allows a straightforward data interpretation within the framework of the neutron scattering theory.[43−46]

The coherent part in eq 1 deals with relative positions of atomic pairs, i.e., collective dynamics:

$$\left(\frac{\partial^2\sigma}{\partial\Omega\partial E}\right)_{coh} = \frac{k}{k_o}\left\langle\sum_{\alpha,\beta}\sum_{i\alpha,\,j\beta}^{N_\alpha N_\beta} b^{\alpha}_{coh}b^{\beta}_{coh}\frac{1}{2\pi\hbar}\int_{-\infty}^{\infty} e^{-i\omega t}\, e^{i\vec{Q}[\vec{r}_{i\alpha}(t)-\vec{r}_{i\beta}(0)]}\, dt\right\rangle \quad (4)$$

Here, $b^{\alpha(\beta)}_{coh}$ is the scattering length of isotopes of the $\alpha(\beta)$ type and $\vec{r}_{i(j)\alpha(\beta)}$ denotes the position of the atom $i(j)$ of the $\alpha(\beta)$ type. The brackets mean thermal average. With all, we can

define a function $I(Q, \omega)$ as

$$\frac{\partial^2\sigma}{\partial\Omega\partial E} = \frac{k}{k_o} I(Q, \omega) \tag{5}$$

that in general contains incoherent and coherent contributions. These are weighed by the total incoherent $\sigma_{inc} = \Sigma_\alpha N_\alpha \sigma^\alpha_{inc}/\Sigma_\alpha N_\alpha$ and coherent $\sigma_{coh} = \Sigma_\alpha N_\alpha \sigma^\alpha_{coh}/\Sigma_\alpha N_\alpha$ cross sections respectively $[\sigma^\alpha_{coh} = 4\pi(b^\alpha_{coh})^2]$.[47] In the case of protonated polymers, and in particular for PES, the double-differential scattering cross section is usually clearly dominated by the incoherent contribution corresponding to the hydrogens in the sample. This is due to the high value of σ^H_{inc} (80.27 barns) as compared to the other scattering cross sections: $\sigma^{C,S,O}_{inc} = 0$, $\sigma^{H,C,S,O}_{coh} < 5.6$ barns. For PES, the ratio between the intensity of the incoherent scattering $\sigma_{inc} = 26.757$ barns/atom (entirely because of its H) and the total scattered intensity $\sigma_{inc} + \sigma_{coh} = 30.693$ barns/atom amounts to 0.872. Therefore, $I(Q, \omega) \propto S^H_{inc}(Q, \omega)$ to a good approximation.

We have to note that as NS spectrometers offer a limited energy resolution, the measured functions are affected by the instrumental resolution function $R(Q, \omega)$. Therefore, the magnitude experimentally accessed is:

$$I_{exp}(Q, \omega) = I(Q, \omega) \otimes R(Q, \omega) \tag{6}$$

$R(Q, \omega)$ is the obtained spectrum when purely elastic ($\hbar\omega = 0$) scattering events take place in the sample [i.e., it is the "image" of $\delta(\omega)$]. It can usually be determined from the scattering of the sample at very low temperature, where all the dynamical processes are frozen and, consequently, $I_{exp}(Q, \omega)$ is proportional to $R(Q, \omega)$. Thus, it can be approximated by:

$$R(Q, \omega) = \frac{I_{exp}(Q, \omega, T \to 0)}{\int_{-\infty}^{\infty} I_{exp}(Q, \omega, T \to 0)\, d\omega} \tag{7}$$

Under the condition of elastic scattering, the modulus of the momentum transfer is simply given by $Q = Q_{el} = 4\pi \sin(\theta/2)/\lambda$, where θ is the scattering angle and λ the wavelength of the incoming neutrons (and, as $E = 0$, also that of the scattered ones). However, when inelastic events take place, neutrons scattered within a given solid angle have experienced different momentum transfers with the sample, depending on the amount of energy interchanged. The relation between scattering angle θ and scattering vector Q turns out to be strongly energy dependent for high values of E.

1. Diffraction with Polarization Analysis. In a diffraction experiment, an integration over all E is performed, and the obtained magnitude is the so-called differential scattering cross section $\partial\sigma/\partial\Omega$.

$$\frac{\partial\sigma}{\partial\Omega} = \int \frac{\partial^2\sigma}{\partial\Omega\partial E} dE = \left(\frac{\partial\sigma}{\partial\Omega}\right)_{inc} + \left(\frac{\partial\sigma}{\partial\Omega}\right)_{coh} \tag{8}$$

In an ideal case, the incoherent contribution in eq 8 is Q-independent, given by $\sigma_{inc}/(4\pi)$, and the coherent contribution reveals the corresponding partial static structure factor (eq 4 with $t = 0$). We note, however, that because of the occurrence of the above-mentioned inelastic events, the integration experimentally performed in the detector (constant angle) of different energy transfers is not identical to the integral at constant Q, which would be the desired result.

If the incoherent scattering arises solely from spin disorder, it flips the neutron spin with probability $^2/_3$, while coherent scattering leaves the spin unchanged. This allows experimental separation of the coherent and incoherent contributions to the scattering by using a spin-polarized neutron beam and polarization analysis (see, e.g., refs 45, 46). With the incident beam polarized ("up"), the number of neutrons scattered within a given solid angle with spin orientations "up" and "down" are:

$$\left(\frac{\partial\sigma}{\partial\Omega}\right)_\uparrow = A\left[\left(\frac{\partial\sigma}{\partial\Omega}\right)_{coh} + \frac{1}{3}\left(\frac{\partial\sigma}{\partial\Omega}\right)_{inc}\right] \left(\frac{\partial\sigma}{\partial\Omega}\right)_\downarrow = A\frac{2}{3}\left(\frac{\partial\sigma}{\partial\Omega}\right)_{inc} \tag{9}$$

where A is a proportionality factor that depends on the experimental conditions (amount of sample in the beam, primary beam intensity, detector efficiencies, etc.). It is worthy of remark that in the absence of inelasticity and multiple scattering, the value of A can easily be obtained from the "down" measurement and the simple calculation of σ_{inc}; then the partial structure factor can be determined in a straightforward way from the "up" measurement in absolute units. The $Q \to \infty$ limit of the coherent differential cross section is $\sigma_{coh}/(4\pi)$.

In this work, we used the diffuse scattering spectrometer D7 at the Institut Laue-Langevin (ILL) in Grenoble (France) on the basis of this principle in its diffraction mode. The incident wavelength was set to 3.1 Å, enabling a range of scattering vectors Q up to 4.0 Å^{-1}. The experiment was performed at 100 K. The correction for background scattering was done by the measurement of the scattering from the empty cell.

2. Time-of-Flight: Microscopic Time Scales. The study on PES dynamics in the microscopic time scale (~0.1−10 ps) was carried out by means of the time-of-flight (TOF) spectrometer G6−2 MIBEMOL at the Laboratoire Léon Brillouin, in Saclay (France). An incident wavelength value of $\lambda = 5.2$ Å was used, yielding an energy resolution δE of $\delta E = 85$ μeV (half width at half-maximum, hwhm). The angular range of the detectors in MIBEMOL is $23.5° \le 2\theta \le 141.8°$, which corresponds to a Q-range of 0.53−2.24 Å^{-1} for elastic scattering at the wavelength used.

The sample (thickness 0.2 mm) was placed into a flat aluminum container and put at an angle of 135° with respect to the incident beam to avoid self-shielding and self-absorption effects. The high value of the transmission of the sample (92.5%) allows the neglect of multiple scattering effects. The measuring times were of ~12 h. We investigated temperatures from 50−450 K every 50 K. The instrumental resolution was determined from a measurement at 10 K. Detector efficiency was corrected by vanadium calibration. The scattering from the sample container was determined at two temperatures and properly subtracted from the spectra. Data corresponding to different detectors were grouped to improve the statistics, resulting in 10 grouped spectra. It is important to note that, as mentioned above, the actual Q-value for one detector strongly deviates from its "elastic" value for energy transfers on the order of some meVs. Therefore, a constant Q-interpolation of the $I_{exp}(\theta, \omega)$ functions to obtain $I_{exp}(Q, \omega)$ was indispensable, leading to a restriction of the energy transfer ranges accessible for small Q-values.

3. Backscattering: Mesoscopic Time Scales. In a backscattering (BS) experiment, perfect crystals are used as monochromators and analyzers, and the instrumental resolution is optimized by using backscattering geometry at both crystals.[48] These spectrometers work under inverse geometry conditions, i.e., the energy of the detected neutrons is fixed to a given value E_f, while the energy of the incident neutrons is varied around E_f. As the energy transfers involved in these experiments are small as compared with the energy of the neutrons, the constant angle spectra correspond to a good approximation to constant $Q = Q_{el}$. In this work, we used the backscattering instrument IN16 at the ILL[49] to explore the mesoscopic time scales (~40 ps to 1 ns).

At IN16, both the monochromator and the analyzers used are made of Si(111) crystals. The energy variation is performed by moving the monochromator and exploiting the Doppler effect. The energy window of the experiment was set to -15 μeV $\le \hbar\omega \le 15$ μeV at an energy resolution of δE(hwhm) $\approx$ 0.4 μeV. Using $\lambda = 6.271$ Å, the data were grouped to have 17 different Q-values in the range between 0.43 and 1.81 Å^{-1}. The flat-shaped sample (thickness 0.35 mm) was positioned at 140° with respect to the incident beam. The temperatures investigated were from 50−400 K every 50, 440, and 480 K. Measuring times were of the order of 12 h. The experimental

resolution function was obtained from a measurement at 10 K. Background corrections were performed for the scattering of the empty cell, which was subtracted with the proper transmission factor. The detector efficiency was corrected by a vanadium measurement. The data reduction was performed by the standard ILL program SQW.

III. Results

A. Incoherent Contribution and Partial Static Structure Factor. Figure 1 shows the differential neutron scattering cross sections of PES obtained by D7. As expected from the values of σ_{inc} and σ_{coh}, the incoherent contribution (originated by the hydrogens in the aromatic rings) is by far the dominant one. It shows a clear Q-dependence due to inelasticity effects that can approximately be described by

$$\left(\frac{\partial\sigma}{\partial\Omega}\right)_{inc} = I_0 \exp\left(-\frac{0.057Q_{el}^2}{3}\right) \qquad (10)$$

In the limit $Q \rightarrow 0$, the incoherent scattering should be entirely elastic, and the prefactor I_0 in eq 10 should coincide with $\sigma_{inc}/(4\pi)$. This has been the criterion adopted to define the absolute scale in Figure 1 [i.e., to determine the value of A in eq 9]. The horizontal dashed line shows the expected incoherent differential cross section in the absence of inelasticity effects. As we will see below, the measured signal in the diffractometer is closer to that obtained when only the elastic scattering is considered.

We now move to the coherent contribution, calculated from eq 9. We observe broad maxima in the partial structure factor, reflecting the amorphous character of the polymer. Considering the values of the scattering lengths and the relative abundance of the different nuclei in the sample, the most strongly highlighted correlations are those corresponding to (C, C) pairs, followed by those between (C, H) and (C, O). The main maximum is located at about 1.3 Å^{-1}, as it is usually found in glass-forming polymers; a second peak centered at ~3 Å^{-1} is also universal for these kinds of systems, and its origin is attributed to intrachain correlations.[50,51] We note that the calculated value of $\sigma_{coh}/(4\pi)$ lies in the range of the average value of the obtained coherent differential cross section and would be a reasonable asymptotic value for its high Q-limit. This supports the consistency of the measurements and the considerations for the estimation of the absolute scale.

Thus, this diffraction study confirms: (i) the glassy character of our sample, and (ii) that the NS signal from protonated PES is practically due to incoherent scattering. Even at the maximum of the partial structure factor, the coherent contribution amounts only to ~20% of the signal. In the complete analysis of the quasielastic data, the coherent contributions will be taken into account, then the information obtained from this D7 study will be used.

B. Microscopic Time Scales. For $Q = 1.12$ Å^{-1}, Figure 2a shows the spectra obtained by means of MIBEMOL for all temperatures investigated. With increasing temperature, the elastic intensity decreases (insert), while in the inelastic and quasielastic regions, the intensity increases. A contribution of vibrational nature is evident for $T \approx 150$ K and below. This feature appears as the well-known Boson peak[52,53] centered at $\hbar\omega \approx 1$ meV. As usually found in glass-forming systems,[52,53] for higher T, the presence of additional

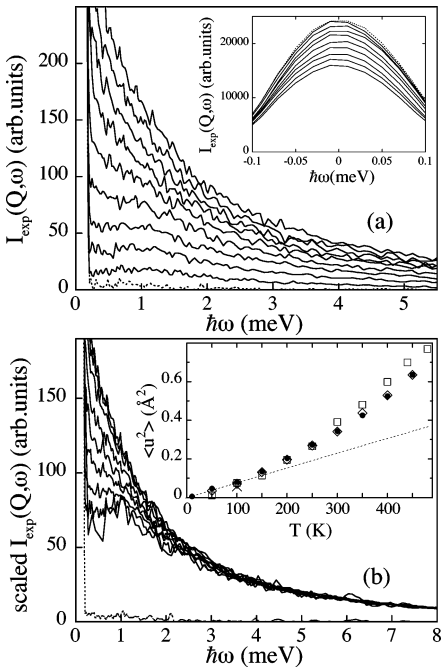

Figure 2. MIBEMOL results on PES. (a) Scattering function at $Q = 1.12$ Å^{-1}. (b) Spectra at $Q = 1.71$ Å^{-1} scaled by the Bose and DWF_{har} factors (reference T: 150 K). The temperatures are: 50, 100, 150, 200, 250, 300, 350, 400, and 450 K (bottom to top). The dotted lines show the resolution function measured at 10 K. Insets: (a) T dependence of the spectra in the elastic region at $Q = 1.12$ Å^{-1} (same temperatures, now from top to bottom). (b) $\langle u^2(T)\rangle$ obtained from the elastic intensities of the MIBEMOL (full circles) and IN16 (squares) spectra and from DWF_{2ps} (diamonds) (see the text). The effective value obtained from the D7 data at 100 K (eq 10) is also shown (cross). The dotted line is a linear regression fit of the MIBEMOL data for $T \leq 150$ K.

intensity is observed, which seems to have a predominantly quasielastic origin.

In the harmonic approximation, the spectra obey the scaling law:

$$S_{inc}^{har}(Q, \omega) = \exp\left(-\frac{\langle u_{har}^2(T)\rangle Q^2}{3}\right)\left[\delta(\omega) + \frac{Q^2}{8\pi M}\frac{g(\omega)}{\omega}[n(\omega)+1]\right] \qquad (11)$$

Here, $\langle u_{har}^2(T)\rangle$ is the mean-squared displacement of the atom around its equilibrium position, $g(\omega)$ the density of states (T-independent in this approximation), $n(\omega) + 1$ the Bose factor ($\propto T$, approximately), and M the atom mass. The decay of the elastic intensity due to harmonic vibrations is thus driven by the harmonic Debye−Waller factor, defined as $DWF_{har} = \exp(-\langle u^2_{har}(T)\rangle Q^2/3)$.

In the general case, a mean-squared displacement $\langle u^2(T)\rangle$ can be deduced by applying an analogous expression to the decay of the measured elastic intensity:

$$DWF_{exp} = \frac{I_{exp}^{el}(Q, T)}{I_{exp}^{el}(Q, T \approx 0)} = \exp\left[-\frac{\langle u^2(T)\rangle Q^2}{3}\right] \qquad (12)$$

We note that the results for DWF_{exp} and $\langle u^2(T)\rangle$ might depend on the instrument considered. If the dynamical process leading to the decay of the elastic intensity takes place at much shorter times than the longest one accessed by the spectrometer, as it is the case of the vibrational modes, the deduced values are independent

of the instrumental resolution, but otherwise (e.g., rotational or diffusive motions) a stronger decrease for the elastic scattering is observed for the higher-resolving instrument. The values for $\langle u^2(T)\rangle$ obtained from the MIBEMOL spectra are displayed in the inset of Figure 2b (full circles). We have plotted here also the "effective" value deduced for this magnitude from the description through eq 10 of the incoherent intensity measured by D7 (cross). It lies slightly below the value obtained from MIBEMOL data at the same temperature. This result is consistent, since on D7, no discrimination in energy transfer is made for the detected neutrons, and therefore, the intensity measured is higher than the purely elastic one, and this might lead to an apparently lower value of $\langle u^2(T)\rangle$. On the other hand, we observe that only for $T \leq 100$ K the T-dependence of $\langle u^2(T)\rangle$ is approximately linear (dotted line), indicating harmonicity. We will consider the values along this dotted line as those characteristic for harmonic vibrations at each T, $\langle u^2_{\mathrm{har}}(T)\rangle$, leading to DWF_{har}. At temperatures close to 150 K and higher, $\langle u^2(T)\rangle$ systematically bends above $\langle u^2_{\mathrm{har}}(T)\rangle$. This indicates the setting up of additional contributions in this temperature range. A higher mobility than that due to pure harmonic vibrations is observed.

To enhance the emergence of nonharmonic contributions, we have scaled the data with the Bose and DWF_{har} factors (eq 11). If the harmonic approximation holds, the scaled spectra should fall into a single curve. As an example, for $Q = 1.71$ Å^{-1}, Figure 2b shows that already at temperatures as low as 150 K, no superposition is achieved. The additional contributions appear in the low-frequency range and are negligible for energies above ~3 meV. Similar features have been found for TOF spectra corresponding to glass-forming systems of different natures during recent years.[52,53] The occurrence of the so-called "fast process" has been invoked to explain this kind of behavior. The origin of such a process is still the subject of debate, and it has been attributed to different phenomena as, for instance, the β-relaxation in the framework of the mode-coupling theory (MCT)[54] or the early stages of the structural relaxation in glass-forming polymers reflecting conformational transitions.[55] The "fast process" would be the mechanism responsible (in addition to the harmonic vibrations) for the decay of the correlations at times below ~2 ps.[56,57]

To deconvolute the spectra from the instrumental resolution and resolve possible additional contributions different from harmonic vibrations and the "fast process", we have Fourier transformed the MIBEMOL spectra to the time domain. The intermediate scattering function has thus been obtained as:

$$S(Q, t) = \frac{\int_{-\infty}^{+\infty} I_{\mathrm{exp}}(Q, \omega, T)\cos(\omega t)\,\mathrm{d}\hbar\omega}{\int_{-\infty}^{+\infty} I_{\mathrm{exp}}(Q, \omega, T \to 0)\cos(\omega t)\,\mathrm{d}\hbar\omega} \quad (13)$$

If the coherent contribution to the scattering can be neglected or if the structure factor does not appreciably change with temperature, this function should be properly normalized, i.e., $S(Q, t = 0) = 1$. Figure 3 shows the result of this deconvolution procedure for $Q = 1.71$ Å^{-1} and the different temperatures investigated and for $T = 400$ K at different Q-values. The main decay of the correlations in this dynamical window takes place at times below ~2 ps, i.e., through vibrations and the "fast process". After this time, the function stays constant for the lowest temperatures, while a smooth decay can be distinguished at high temperatures. Taking into account that the sample is in the glassy state, the process leading to the decay of the correlations at $t \geq 2$ ps should be related to localized motions, probably contributing to some of the secondary relaxations identified in these kinds of systems.

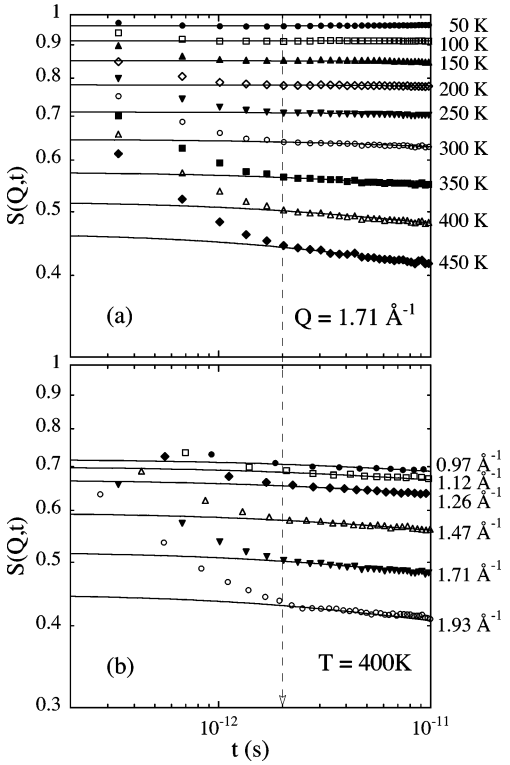

Figure 3. Intermediate scattering function of PES at $Q = 1.71$ Å^{-1} for different temperatures (a) and at $T = 400$ K for different Q-values (b). The continuous lines are the descriptions obtained with the proposed model, for which a short time limit is indicated by the vertical dashed arrow.

Since the full characterization of the dynamics leading to the decay of the correlations at $t \leq 2$ ps is beyond the scope of this work, we will consider the contribution of this global fast process as a prefactor for the function describing the temporal evolution of the correlations at longer times. This prefactor, that we will consider the "effective" DWF, can be taken in a first approximation as the value of $S(Q, t)$ at $t = 2$ ps, $DWF \approx DWF_{2\mathrm{ps}} = S(Q, t = 2\ \mathrm{ps})$. The mean-squared displacement associated with this fast motion is very close to that obtained from the decay of the elastic intensity in MIBEMOL [see diamonds in the insert of Figure 2b]. This reflects the fact that almost the totality of the dynamics observed in this window is driven by the fast motional processes parametrized by the DWF. Any further decrease of the DFW_{exp} obtained in other dynamical windows with better resolution has to be associated with slower relaxations. We note at this point the importance of the DWF in the NS measurements, since it reduces the amplitude of the decay of the correlations (equivalently, the amplitude of the signal, both elastic and quasielastic, of the spectra in the frequency domain) for any process slower than the fast motion causing the DWF.

Because of the weakness of the decay observed between $t \geq 2$ ps and the limit imposed by the TOF resolution, it is advisable to scrutinize the T- and Q-dependencies of $S(Q, t)$ in terms of the following

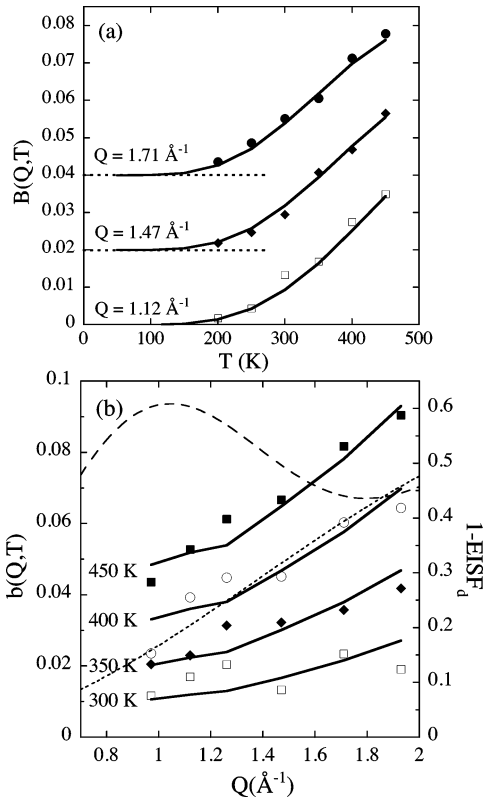

Figure 4. (a) T-dependence for selected Q-values of $B(Q, T)$ (eq 14) and (b) Q-dependence of $b(Q, T) = B(Q, T)/DWF$ for the indicated temperatures. Solid lines show the results of the model proposed. For clarity, the data corresponding to 1.47 and 1.71 Å^{-1} in (a) have been shifted by 0.02 and 0.04, respectively, and the horizontal dotted lines show their "0" level. For comparison, the modulation of the quasielastic intensity determined by $(1 - EISF_d)$ is displayed in (b) for two values of the jump distance: $d = 4.3$ Å (dashed) and $d = 1.5$ Å (dotted line).

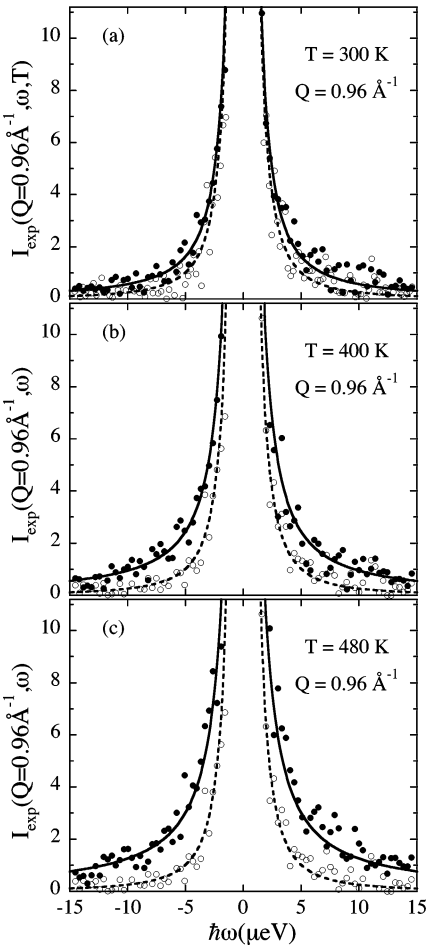

Figure 5. IN16 spectra obtained for PES at $Q = 0.96$ Å^{-1} and 300 (a), 400 (b), and 480 K (c) (solid circles). The 10 K data are also shown (empty circles). The dotted line is a description of the low T-data with a Lorentzian plus a Gaussian function. Solid lines show the descriptions in terms of the model proposed. The maximum of the scale is the 1% of the maximum value of the 10 K spectrum.

function: the apparent slope of $S(Q, t)$ with respect to the variable log$t$ in such time interval,

$$B(Q, T) = \left|\frac{\mathrm{d}S(Q, t)}{\mathrm{d}\log t}\right|_{t>2\mathrm{ps}} \qquad (14)$$

This function is very sensitive to the appearance of dynamical processes in the dynamical window. Figure 4a shows the T-dependence of $B(Q, T)$ obtained from PES $S(Q, t)$ data. From it, an incipient contribution of the relaxational process can be noticed at $T \approx 200$ K that increases with T. Dividing by the DWF, the influence of the existence of the first decay in $S(Q, t)$ is removed; therefore, we have displayed in Figure 4b the function $b(Q, T) = B(Q, T)/DWF_{2\mathrm{ps}}$ as a function of Q. We observe that $b(Q, T)$ monotonically increases with increasing Q in the Q-range accessible in this TOF investigation.

C. Mesoscopic Time Scales. Figure 5 shows that for Q-values close to 1 Å^{-1} a clear quasielastic broadening can be observed in the IN16 spectra at $T \approx 300$ K and above. The quasielastic intensity increases with increasing T. Moreover, at constant temperature, it shows a maximum at around $Q \approx 1$ Å^{-1} (see Figure 6). We have to note that, though detectable, the quasielastic intensities are quite weak. In both figures, the scales have been displayed at 1% of the intensities at the maxima of the resolution spectra. Therefore, despite the long measuring times employed, the data in the quasielastic region might show a relatively high dispersion.

The Q- and T-dependencies of the intensities, especially of the quasielastic ones, can be better appreciated if integrals of the spectra are calculated:

$$I_{\Delta\hbar\omega}(Q, T) = \int_{\Delta\hbar\omega} I_{\mathrm{exp}}(Q, \omega, T)\, \mathrm{d}\hbar\omega \qquad (15)$$

We have obtained this function for different energy windows on IN16. For $|\Delta\hbar\omega| \leq 0.4$ μeV, eq 15 delivers the elastic intensity $I_{\mathrm{el}}^{\mathrm{IN16}}(Q, T)$. Its T-dependence is shown in Figure 7 for different Q-values. The observation that its values for $T \to 0$ do not exactly coincide is due to the contribution of coherent scattering to the spectra; this is consistent with the D7 results. The description of the decay of the elastic intensity in terms of eq 12 leads to the values for the mean-squared displacement shown in the inset of Figure 2b. The slightly higher values obtained from the BS instrument with respect to those deduced from the TOF spectrometer for $T \approx 300$ K and above indicate the occurrence at these temperatures of dynamical processes with characteristic time scales intermediate between the resolution of both instruments.

For $2\ \mu\mathrm{eV} \leq |\Delta\hbar\omega| \leq 5\ \mu\mathrm{eV}$, we obtain from eq 15 what we will call $I_{\mathrm{Qel1}}^{\mathrm{IN16}}(Q, T)$. Its T-dependence is shown in

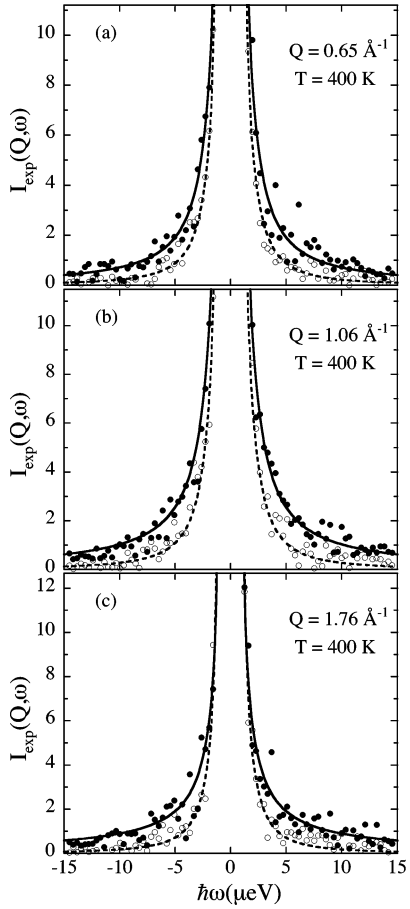

Figure 6. IN16 spectra obtained for PES at 400 K (full circles) and 10 K (empty circles) for $Q = 0.65$ Å^{-1} (a), $Q = 1.06$ Å^{-1} (b), and $Q = 1.76$ Å^{-1} (c). Lines as in Figure 5. The scales are shown at the 1% of the maximum values of the respective 10 K data.

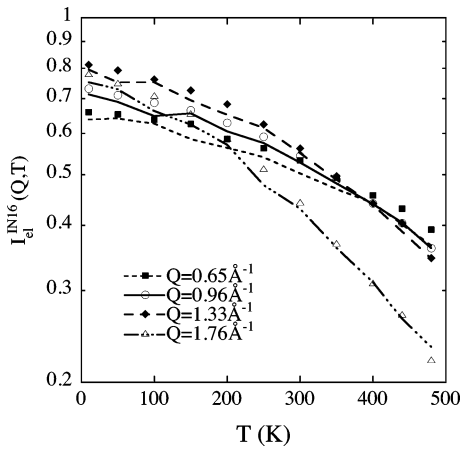

Figure 7. *T*-dependence of the elastic intensities obtained from IN16 for the *Q*-values indicated. The lines show the results of the model proposed.

Figure 8 for different *Q*-values. While for the lower *Q*-values, $I_{Qel1}^{IN16}(Q, T)$ monotonically increases with *T*, at the highest *Q*'s, a sort of plateau is found after an increase between 200 and 300 K. This plateau reflects the strong influence of the *DWF* at high *Q*-values. As it was done for $B(Q, T)$ in Figure 4b, the renormalization by division with the *DWF* removes the decay of the intensity in the spectra because of the occurrence of the fastest processes below ~2 ps. This procedure leads to the results displayed in Figure 9. At first sight, a

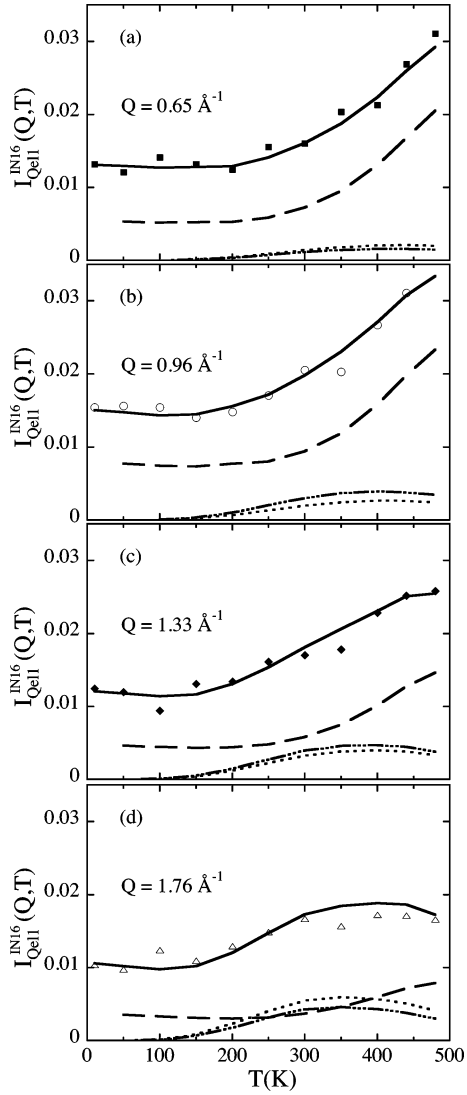

Figure 8. *T*-dependence of the quasielastic intensities obtained from IN16 for $2\ \mu eV \le |\Delta\hbar\omega| \le 5\ \mu eV$ for $Q = 0.65$ Å^{-1} (a), 0.96 Å^{-1} (b), 1.33 Å^{-1} (c), and 1.76 Å^{-1} (d). Solid lines show the results of the model proposed; the contributions from the flips, oscillations, and mixed term are displayed as dashed, dotted, and dashed−dotted lines, respectively.

striking feature is found from this figure: for the highest temperatures, $I_{Qel1}^{IN16}(Q, T)/DWF$ shows a marked peak in the *Q*-range ~1 Å^{-1}. However, at $T \approx 200$ K, the highest quasielastic contributions seem to occur at the highest *Q*-values accessible by this instrument. The same features pointed out for $I_{Qel1}^{IN16}(Q, T)$ can be found in the quasielastic region corresponding to higher-energy transfers. This is shown in Figure 10, where $I_{Qel2}^{IN16}(Q, T)$ calculated for $-15\ \mu eV \le |\Delta\hbar\omega| \le -5\ \mu eV$ is displayed as a function of both variables, *T* (a) and *Q* (b). The overall observations made considering both instruments, IN16 and MIBEMOL, point then to the presence of at least two different relaxational processes involving different geometrical features.

Thus, the dynamical behavior of aromatic hydrogens in glassy PES seems to show a certain degree of complexity. To describe it, a model recently developed for phenylene ring dynamics in BPA-PSF[36] will be applied. It is presented in the next section.

IV. Model for Phenylene Ring Dynamics

A. Proposed Scenario. The occurrence of π-flips of the phenylene rings in aromatic polymers such as PES

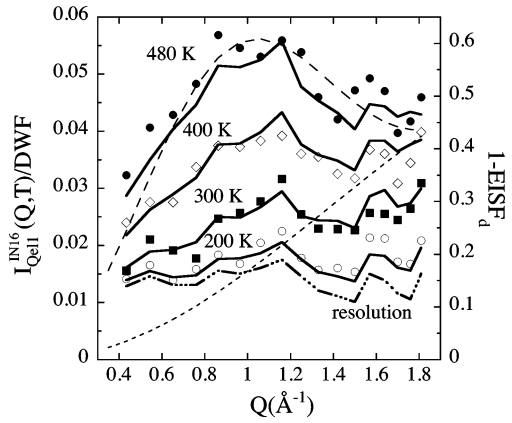

Figure 9. Q-dependence of the quasielastic intensities obtained from IN16 for 2 μeV $\leq |\Delta\hbar\omega| \leq$ 5 μeV and divided by DWF$_{2ps}$ at 200, 300, 400, and 480 K (symbols, bottom to top). Dashed−dotted line represents the intensity of the resolution function (low T-data). Solid lines show the results of the model proposed. For comparison, the modulation of the quasielastic intensity determined by $(1 - EISF_d)$ is displayed for d = 4.3 Å (dashed) and d = 1.5 Å (dotted line).

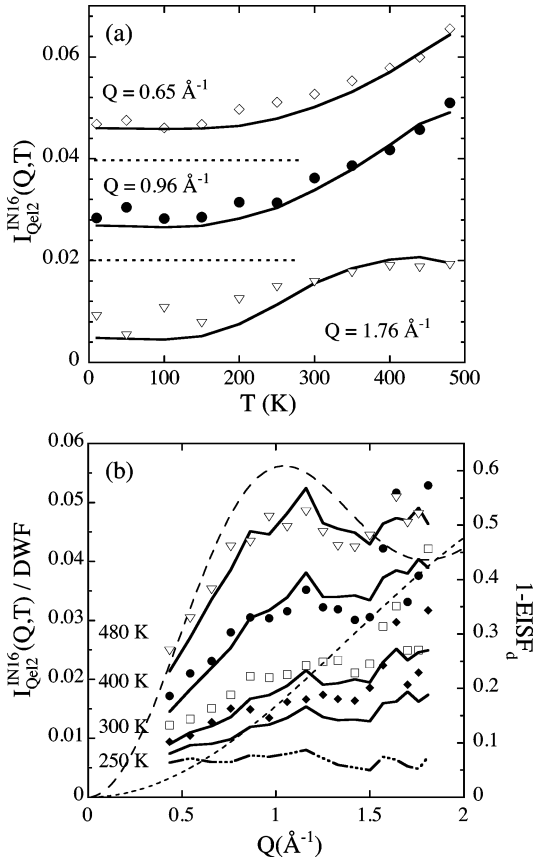

Figure 10. (a) T-dependence for selected Q-values of the quasielastic intensities obtained from IN16 for 5 μeV $\leq |\Delta\hbar\omega| \leq$ 15 μeV and (b) Q-dependence of the same quantities divided by the *DWF* for the indicated temperatures. Solid lines show the results of the model proposed. For clarity, the data corresponding to 0.96 and 0.65 Å^{-1} in (a) have been shifted by 0.01 and 0.02, respectively, and the horizontal dotted lines show their "0" level. For comparison, the modulation of the quasielastic intensity determined by $(1 - EISF_d)$ is displayed in (b) for d = 4.3 Å (dashed) and d = 1.5 Å (dotted line). The dashed−dotted line represents the intensity of the resolution function (low T-data).

has been repeatedly invoked in the literature from NMR[16−25] and molecular mechanics calculations.[26−35] Recent NS studies on BPA-PSF,[36,38] BPA-PC,[39,40,58] and PH[58] reveal such flips as well. As NS follows aromatic hydrogen dynamics, the manifestation of this motion consists of a jump of the proton over a distance of 4.3 Å.

For the general case of jumps of an atom between two equivalent sites separated by a distance d, the incoherent scattering function can be expressed as:[43,44]

$$S^d_{\mathrm{inc}}(Q, t) = EISF_d + (1 - EISF_d)\exp\left(-\frac{t}{\tau_d}\right) \quad (16)$$

or, in the frequency domain, as:

$$S^d_{\mathrm{inc}}(Q, \omega) = EISF_d\delta(\omega) + (1 - EISF_d)\frac{1}{\pi}\frac{\tau_d}{1 + (\omega\tau_d)^2} \quad (17)$$

The label "d" refers to the nature of the motion considered (until now, it designates a generic jump over a such a distance). Here, τ is the characteristic time [$1/(2\tau_d)$ is the transition rate], usually T-dependent but Q-independent because of the localized nature of the motion. For thermally activated processes it follows an Arrhenius-like dependence

$$\tau_d(T) = \tau_o \exp\left(\frac{E^d_a}{k_B T}\right) \quad (18)$$

with $\tau_o \approx 10^{-13}$ s, E^d_a the corresponding activation energy and k_B the Boltzmann constant. The so-called elastic incoherent structure factor $EISF_d$ determines the elastic intensity and carries the information on the geometry of the motion. In the case considered here of two site jumps, it is given by:

$$EISF_d = \frac{1}{2}\left[1 + \frac{\sin Qd}{Qd}\right] \quad (19)$$

$EISF_d$ is an oscillatory function around 0.5 with the first minimum located at $Q = 3\pi/2d$. In a complementary way, $(1 - EISF_d)$ modulates the quasielastic intensity [see eq 17] and also the log t-derivative of the intermediate scattering function, i.e., what we have defined as $B(Q, T)$. In the general case, the total scattering function has, in addition, the *DWF* on the top.

For a π-flip of the ring, the first minimum of $EISF_d$ happens at $Q \sim 1$ Å^{-1} for the hydrogen-scattering function. There, the quasielastic intensity, once the *DWF* influence is removed, should show its maximum value. Can such a type of motion be inferred from our experimental results in the different windows?

The high-temperature data collected on IN16 indisputably mirror the occurrence of such a π-flip of the rings (see Figures 9 and 10b). This is, however, clearly not the case for the data in the microscopic window. Figure 4 shows that the variation of $b(Q, T)$ with Q does not resemble the $(1 - EISF_d)$ for a π-flip of the ring at all, but rather that corresponding to a jump over a much shorter distance, $d \approx$ 1.5 Å. This would indicate a motion more restricted in space than the π-flip of the ring. Coming back to IN16 and focusing on low temperatures, the difference of the quasielastic intensity relative to the resolution signal seems also to monotonically increase toward high Q-values, reminiscent of the Q-dependence observed in the microscopic window [see Figures 9 and 10b].

Thus, from the scrutiny of the experimental results, the need to consider a third kind of movement for the aromatic hydrogens, apart from the fast processes and the π-flips of the rings, becomes imperative. Such motion would lead mainly to the decay of the intermediate scattering function in the MIBEMOL dynamic window above 2 ps, though it can also be detected at relatively low temperatures on IN16. From these observations and the Q-dependence found, it should correspond to a motion involving the rings with characteristic times intermediate between the fast processes and the π-flips and with smaller amplitude than the last. Thus, all these three motions have to be considered to reproduce the experimental observations.

In our scenario, we consider the combined occurrence of π-flips and small-amplitude oscillations (characterized by the rotational angle ϕ) of the rings around their equilibrium positions. The motion of the hydrogen that what we follow with NS is the consequence of these two ring motions and the rapid vibrations and other fast processes contributing at very short times. Our first assumption is to consider that the decay of the correlations through the fast processes can be effectively described above 2 ps by an effective *DWF*. The second one is to assume the two ring motions as statistically independent processes. Then the scattering function of a given hydrogen for $t \geq 2$ ps reads:

$$S_{\mathrm{inc}}(Q, t) = DWF \cdot S^{\pi}_{\mathrm{inc}}(Q, t) \cdot S^{\phi}_{\mathrm{inc}}(Q, t) \qquad (20)$$

The scattering functions $S^{\pi}_{\mathrm{inc}}(Q, t)$ and $S^{\phi}_{\mathrm{inc}}(Q, t)$ are given by eq 16 with eq 19, where for the case of the π-flips $d = 4.3$ Å and for the oscillations $d = 2\sin(\phi/2)$. This leads to the following expression:

$$S_{\mathrm{inc}}(Q, t) = S_{\mathrm{el}}(Q) + S_{\mathrm{Qel}\pi}(Q, t, \tau_{\pi}) + S_{\mathrm{Qel}\phi}(Q, t, \tau_{\phi}) + S_{\mathrm{Qel}\pi\phi}(Q, t, \tau_{\pi}, \tau_{\phi}) \qquad (21)$$

where the elastic and quasielastic contributions are defined as:

$$S_{\mathrm{el}}(Q) = DWF \cdot EISF_{\pi} \cdot EISF_{\phi} \qquad (22)$$

$$S_{\mathrm{Qel}\pi}(Q, t, \tau_{\pi}) = DWF\left[(1 - EISF_{\pi})EISF_{\phi} \exp\left(-\frac{t}{\tau_{\pi}}\right)\right] \qquad (23)$$

$$S_{\mathrm{Qel}\phi}(Q, t, \tau_{\phi}) = DWF\left[(1 - EISF_{\phi})EISF_{\pi} \exp\left(-\frac{t}{\tau_{\phi}}\right)\right] \qquad (24)$$

$$S_{\mathrm{Qel}\pi\phi}(Q, t, \tau_{\pi}, \tau_{\phi}) = DWF\left[(1 - EISF_{\pi})(1 - EISF_{\phi}) \exp\left(-\frac{t}{\tau_{\pi}}\right) \exp\left(-\frac{t}{\tau_{\phi}}\right)\right] \qquad (25)$$

Figure 11 shows as an example the Q-dependence of the quasielastic contributions in comparison with those corresponding to the simple motions. We observe that the mixed term shows similar strength to that of the oscillations. We note that such a term is a consequence of the assumption of statistically independent processes and would reflect in some way how one of the motions is altered by the occurrence of the other. On the other hand, the characteristic time for each of the motions (τ_{π}, τ_{ϕ}) would obey the Arrhenius law (eq 18) with the respective activation energy (E^{π}_{a} and E^{ϕ}_{a}); there, both

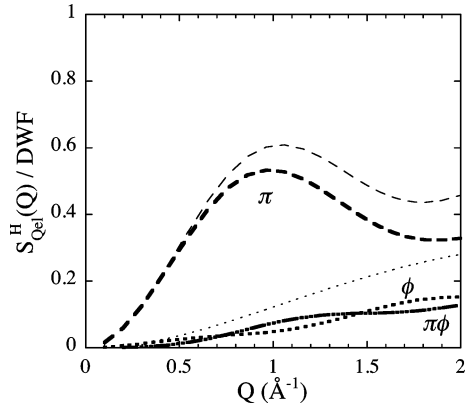

Figure 11. Quasielastic intensities (*DWF* corrected) of the contributions corresponding to the π-flips (eq 23, dashed thick line), oscillations (eq 24, dotted thick line), and mixed term (eq 25, dashed−dotted line) in the model. The thin lines show the equivalent intensities for the individual motions. For the oscillations, the function corresponding to the obtained results for 440 K has been chosen.

prefactors have been assumed to be 10^{-13} s. We point out that, in the proposed scenario, the apparent activation energy for flips would represent a real potential barrier over which the phenylene ring jumps. In contrast, oscillations would take place (probably correlated with other fast motions with small associated spatial scales) as a result of rapid fluctuations of the single particle potential seen by the phenylene ring and produced by the surrounding atoms. In this case, the apparent activation energy for oscillations would only reflect the characteristic time of such fluctuations.

At this point, we add to the model the essential ingredient of the disorder present in glassy systems. Nowadays, it is well-known that the packing heterogeneity characteristic for the amorphous character of polymers leads to broad distributions of the dynamical parameters. A clear example is the distribution appearing for rotational barriers in methyl groups that leads to well-known classical and quantum effects.[59−62] Here, the fact that (at least) the oscillation motion contributes in the same temperature range (around and above 200 K) to both dynamical windows indicates that such broad distributions have to be present.

Depending on the local packing, the contribution of the intermolecular interactions to the local potential seen by an atom or group of atoms would vary from point to point. Different local potentials would lead to different characteristic times for a particular motion. As a consequence, the incoherent scattering reflects the heterogeneity in the system and will be given by the sum of several scattering functions coming from different environments holding different characteristic times

$$S_{\mathrm{inc}}(Q, t) = \sum_{k} p_{\mathrm{k}} S^{\mathrm{k,H}}_{\mathrm{inc}}(Q, t) \qquad (26)$$

where $\Sigma_k p_{\mathrm{k}} = 1$, and each of the $S^{\mathrm{k,H}}_{\mathrm{inc}}(Q, t)$ functions is defined as in eq 20. The index k determines the characteristic times of the motions performed by the atom, as we will see below. The weight p_{k} would be determined by the distribution of a certain undefined structural parameter ξ driving the single particle dynamics

$$p_{\mathrm{k}} = \int_{\delta\xi} g(\xi)\, \mathrm{d}\xi \qquad (27)$$

The relation between ξ and the local potential defining the characteristic time of the motion would be different for different motions depending on their specific nature, since some motions are more influenced by inter/intramolecular interactions than others. As a consequence, the functional relation between ξ and the local potential for oscillations and between ξ and the local potential for flips might not be the same. In any case, if the characteristic time of the motion in a certain local environment is parametrized by an activation energy E_a^d (where d corresponds to either ϕ or π), the activation energies will be distributed as well (via eq 18) as a result of the intermolecular packing, so that

$$p_k = \int_{\delta E_a^\phi} h_\phi(E_a{}^\phi)\mathrm{d}E_a^\phi = \int_{\delta E_a^\pi} h_\pi(E_a^\pi)\,\mathrm{d}E_a^\pi \qquad (28)$$

The interpretation of the distribution in eq 26 in terms of packing effects implies that long characteristic times for flips occur in a local environment with long characteristic times for oscillation, and otherwise, short characteristic times for flips occur together with short characteristic times for oscillations. That is, although the two motions have been considered statistically independent, the activation energies for both motions in a certain local environment are assumed to be correlated.

B. Application to the NS Results. To compare the model function with the experimental data, several considerations have to be made. First of all, in addition to the incoherent scattering from the aromatic hydrogens, the measured scattering contains other contributions that have to be taken into account. As mentioned above, these are purely coherent, and their global amount has been characterized by D7. Since motions yielding identical initial and final atomic configurations, as in the case of the π-flips, do not give rise to coherent quasielastic scattering, we may consider in a first approximation that the coherent contribution to the spectra is just elastic and assume for it the same *DWF* as the incoherent scattering of the aromatic hydrogens. Then, the model function has an additional elastic contribution weighed by *DWF* and the partial structure factor. In the frequency domain at mesoscopic scales, the whole model function reads as:

$$I_{\mathrm{model}}(Q,\omega) = \sum_\alpha N_\alpha\left[\frac{\sigma_{\mathrm{inc}}}{4\pi}S_{\mathrm{inc}}^{\mathrm{H}}(Q,\omega) + \left(\frac{\partial\sigma}{\partial\Omega}\right)_{\mathrm{coh}} DWF\,\delta(\omega)\right] \qquad (29)$$

and has to be convoluted with the resolution function (eq 6) to be compared with the experimental IN16 results. To prevent dispersion, an analytical approach to $R(Q,\omega)$ is used. It consists of the addition of a Gaussian and a Lorentzian function that provides a good description of the low-temperature experimental data shown in Figures 5 and 6 (dotted lines). On the other hand, and in an analogous way, the Fourier transform of eq 29 to the time domain normalized to its static value is to be compared with the experimental $S(Q,t)$ obtained from the TOF data through eq 13. We recall that the range of validity of the model function is restricted to $t \geq 2$ ps. In addition to the proper scattering functions, we have calculated the predictions for the quantities in terms in which the main features of the dynamics have been characterized: $B(Q,T)$ for $t \geq 2$ ps in the TOF window and the different integrated intensities in the IN16 window.

Though at first sight a large number of parameters seem to be involved in the model function, most of them are actually fixed or known from the D7 measurements. Apart from refining the *DWF* values, the distribution functions of activation energies for both processes, $h_\pi(E_a^\pi)$ and $h_\phi(E_a^\phi)$, and the geometry of the motion involved in the oscillations are to be determined. For the activation energies of the π-flips, a Gaussian distribution with average value $\langle E_a^\pi\rangle$ and variance σ_π was assumed:

$$h_\pi(E_a^\pi) = \frac{1}{\sqrt{2\pi}\sigma_\pi}\exp\left[-\frac{(E_a^\pi - \langle E_a^\pi\rangle)^2}{2{\sigma_\pi}^2}\right] \qquad (30)$$

Since a symmetric distribution of $E_a{}^\phi$ extends to negative values of E_a^ϕ, we have used a two-parameter (m and the average E_a^ϕ, $\langle E_a^\phi\rangle$) asymmetric distribution function for E_a^ϕ,

$$h_\phi(E_a^\phi) = \frac{m^m}{\langle E_a^\phi\rangle\Gamma(m)}\left(\frac{E_a^\phi}{\langle E_a^\phi\rangle}\right)^{m-1}\exp\left(-m\frac{E_a^\phi}{\langle E_a^\phi\rangle}\right) \qquad (31)$$

where $\Gamma(m)$ is the Gamma function. The so-defined $h_\phi(E_a^\phi)$ is zero for $E_a^\phi < 0$.

Concerning the geometrical parameters involved in the oscillations, we have assumed that the associated amplitudes are distributed around an average value (that in principle could be temperature dependent) according to a Gaussian function:

$$g_\phi(\phi) = \frac{2}{\pi\langle\phi\rangle}\exp\left[-\frac{1}{\pi}\frac{\phi^2}{\langle\phi\rangle^2}\right] \qquad (32)$$

where by definition the oscillation angle ϕ assumes only values between 0 and π. No coupling between energy and amplitude of motion was assumed.

The determination of the values of the fitting parameters ($\langle E_a{}^\pi\rangle$, σ_π, m, $\langle E_a^\phi\rangle$, and $\langle\phi\rangle(T)$) was possible by the following procedure:

- A first approach to the parameters corresponding to the oscillations is obtained by using the TOF information. No maximum is visible at $Q \approx 1$ Å^{-1} for $b(Q,T)$ (Figure 4). This implies that in the T-range investigated, the π-flip contributions are still too weak to be detected in the TOF window. If we consider the highest Q-value accessible by these measurements ($Q = 1.93$ Å^{-1}), it is even less probable to observe any π-flip contribution since the function $S_{\mathrm{Qel}\pi}(Q)$ [mirroring $(1 - EISF_\pi)$, see eq 23] reaches a minimum for this Q-value [see Figures 4b and 11]. Then, m, $\langle E_a^\phi\rangle$, and $\langle\phi\rangle(T)$ can be fitted by considering that the only process that causes the decay of the intermediate scattering function under these conditions are the oscillations. The value for $\langle\phi\rangle(T)$ could only be determined for the two highest temperatures investigated, and the consequent linear extrapolation was used for lower temperatures.
- Turning to the mesoscopic window, for the highest temperatures, the strongest contribution is that of the π-flips [see the maximum intensity close to $Q \approx 1$ Å^{-1} in Figures 9 and 10b]. By thus neglecting the oscillations contribution at these temperatures in the Q-region close to 1 Å^{-1}, a first approach to the values of $\langle E_a^\pi\rangle$ and σ_π can be obtained.

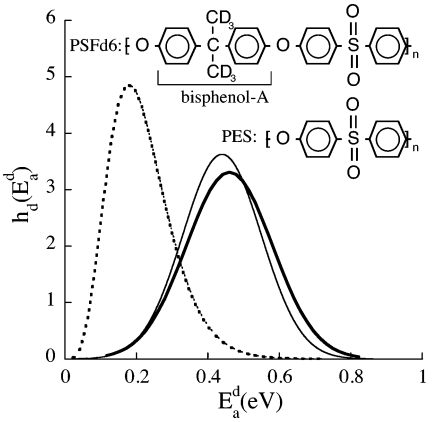

Figure 12. Distribution functions of activation energies for oscillations (dotted lines) and π-flips (solid lines) of phenylene rings obtained for PES (thick lines) and BPA-PSF with deuterated methyl groups (PSFd6) (thin lines).[36,37] The chemical structures of both polymers are also shown.

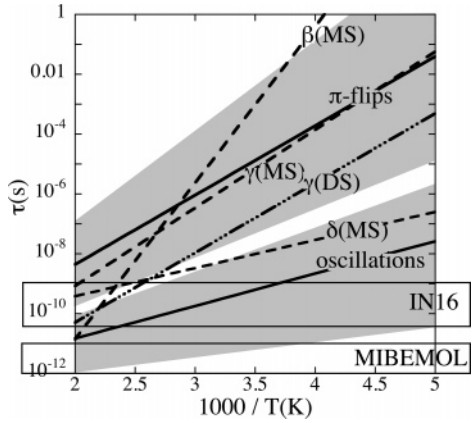

Figure 13. Temperature dependence of the characteristic (average) times obtained from this study for the two motions identified for PES phenylene rings, oscillations, and π-flips (solid lines). The shadowed areas around them represent the width of the distributions (regions of characteristic times corresponding to energies for which the distribution functions present values higher than their half maxima). The characteristic times deduced from mechanical spectroscopy for the three relaxations observed by L. David et al.[8] are displayed for comparison as dashed lines and those obtained from dielectric spectroscopy as a dashed−dotted line. The rectangles delimit the dynamical regions explored by the NS spectrometers in this work.

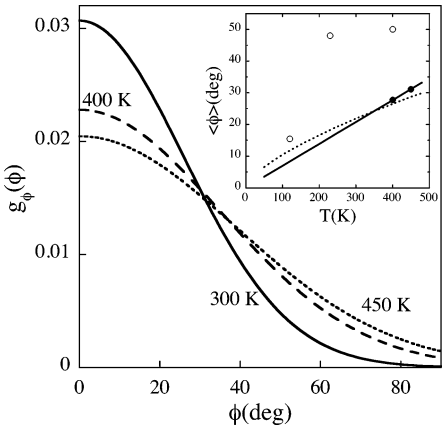

Figure 14. Distribution functions of oscillation angles at the three temperatures indicated. The insert shows the temperature dependence obtained for the width of the distribution (full circles); the solid line through the points is a linear regression fit. The dotted line shows the T-dependence used in the case of BPA-PSF.[36,37] The empty circles show the average amplitude of rotational angles obtained from the populations of rotational angles around their average values from the MD simulations of Shi et al.[71]

- Once the two motions are characterized in an independent way, the whole scattering function is considered and the parameters are refined by comparison with the experimental results for all Q-values and temperatures investigated in each window. First, in the microscopic window, tuning also the *DWF*, and thereafter, in the mesoscopic window. This step is repeated until a stable set of values for the parameters is achieved.

This refinement procedure only led to a minor change in the values of the initial parameters. A maximum error of 5% for the values obtained can be estimated. The values finally obtained were: $\langle E_a^{\pi}\rangle = 0.46$ eV and $\sigma_\pi = 0.12$ eV for the energy distribution of π-flips, $\langle E_a^{\phi}\rangle = 0.215$ eV, and $m = 6$ for that of oscillation energies (corresponding to a hwhm of 0.095 eV) and $\langle\phi\rangle(T)$[rad] $= 0.0691T$[K] ($\langle\phi\rangle(450\text{ K}) = 31°$, $\langle\phi\rangle(400\text{ K}) = 28°$). Figure 12 displays the corresponding distribution functions of activation energies. They give rise to temperature-dependent distributions of characteristic times, for which the average values are plotted in Figure 13 as solid lines. To give an idea of the width of these functions, we have shaded in this Arrhenius plot the areas covering the time scales corresponding to the most probable characteristic times; the criterion adopted was to consider the region of energies where $h_d(E_a^d)$ ($d \leftrightarrow \pi$, ϕ) shows values higher than its half-maximum. Finally, Figure 14 shows the distribution functions of angles of oscillation for three temperatures.

V. Discussion

Within the range of applicability of the model proposed ($t \geq 2$ ps), a very good agreement is found between its predictions and experiment. In the microscopic window, the model function perfectly describes the decay of the intermediate scattering function for the different Q-values and temperatures investigated (see Figure 3). Consequently, the T- and Q-dependences of the calculated slopes $B(Q, T)$ are fairly reproduced, as can be appreciated in Figure 4. Only a small discrepancy might be found for $Q \approx 1.3$ Å^{-1}, where the theoretical value for $b(Q, T)$ is systematically smaller than that of the experimental one. We will come later to this point. With all, we can claim that our model delivers a very satisfactory description of the microscopic data. On the other hand, the model also captures all the features shown by the mesoscopic results, as shown in Figures 5−10.

In the following, we analyze the contributions of the different processes in the two dynamic windows investigated. Starting with the microscopic window, most of the decay of the correlations there (correspondingly, most of the quasielastic/inelastic intensity in the TOF window) is due to the "fast processes" parametrized by the *DWF*. As already mentioned, the origin of this process is still a matter of strong debate. In seeking a plausible molecular picture of this process, we could think that it comprises some motions the hydrogen performs relative to the carbon to which it is linked. Such contributions can be inferred from the comparative study of the microscopic dynamics of C and H from MD-simulations.[63] Also, the interpretation of NMR spectra

in different polymers required the consideration of some kind of fast librations.[64−70] In those works, anisotropic reorientations occurring with a fast correlation time inside a cone of half-angle θ, the axis of which is the rest position of the CH bond, were assumed. Values between 20° and 40° were obtained for θ, depending on the type of H and polymer investigated. A correlation between this angle and the steric hindrance was found; furthermore, as identical amplitudes were observed in bulk and solution, an entirely intramolecular origin was deduced for this reorientation. The spatial extent of the fast motions observed by NS is revealed by $\langle u^2(T)\rangle$ [see insert in Figure 2b]. The values obtained for PES would lead in this kind of scenario to a cone semiangle for H-librations of $\theta \approx 33°$ at room temperature, compatible with those values reported so far from the NMR studies. On the other hand, the associated characteristic time would be in fact very fast, on the order of ∼0.3 ps (see Figure 3).

Still within the microscopic window, let us now turn to longer times (above 2 ps). From Figure 13, it becomes clear that in the whole T-range investigated, the π-flips are much too slow to be detected in the MIBEMOL window and basically only oscillations are active there. Even for these faster motions, the average time of the distribution function does not become fast enough to match the TOF window below T_g. The observed decay for the intermediate scattering function above 2 ps is thus due to the fastest oscillations of the rings [low-energy wing of $h_\phi(E_a^\phi)$]. At this point, we note that for oscillations of the rings with amplitudes as those we have obtained ($\langle\phi\rangle \approx 20°..0.30°$), the coherent contribution is not purely elastic anymore as it was assumed and contributes to increase the slope of the intermediate scattering function. This explains the small discrepancy between model and experiment observed for $b(Q, T)$, close to the first maximum of the partial structure factor.

The mesoscopic window is sensitive to both oscillations and π-flips (see Figure 13), their respective visibilities being distinctly highlighted in different Q- and T-ranges. From Figure 11, we can deduce that the π-flips still dominate the quasielastic signal in the Q-range around 1 Å^{-1}, while in the highest Q-region, the contributions of all three terms (π-flips, oscillations, mixed) are important. In the measured spectra, the intensities of the different contributions are of course affected also by the dynamic terms (intensity of the corresponding Lorentzians), which vary with temperature, reflecting how the time scales of the processes enter in the dynamic window of IN16. In Figure 8, we have plotted the different contributions to the quasielastic intensity corresponding to the three terms in eqs 23, 24, and 25. The oscillations and mixed term dominate at low temperatures, showing a broad maximum for the intensity at about 400 K (this maximum is apparently shifted toward lower temperatures at high Q-values because of the influence of the *DWF*). This behavior reflects that around this temperature the distribution of relaxation times is centered in the instrumental window. We observe that the mixed contribution shows similar importance to that of the oscillations, a signature of the fact that the relaxation times associated to the π-flips are quite slow and the dynamic contribution to the mixed term is most influenced by the oscillations. Finally, we can see that above ∼400 K, the π-flips take the dominant role in the quasielastic contribution.

It thus becomes clear that the combination of different NS spectrometers accessing both dynamic windows is imperative to fully describe the dynamics of phenylene rings in these systems; this is due not only to the occurrence of more than one single motion but also to the broad character of the distribution functions of relaxation times.

Now we discuss in detail the two motions observed for PES rings. The occurrence of π-flips of phenylene rings in a large number of aromatic polymers has been repeatedly reported from NMR studies. For different polycarbonates,[16,17,20−22] broadly distributed associated characteristic times with a mean activation energy of 0.52 eV have been found. A similar T-dependence is reported for phenoxy[25] and a series of epoxy resins.[24] Finally, NMR investigations on poly(arylene ether sulfones)[19] and PEEK[23] show also the existence of phenylene π-flips. Although to our knowledge, no NMR results on PES phenylene ring dynamics have yet been published, we note that the value obtained in this work for the activation energy of the π-flips is similar to those reported from NMR for the other systems. On the other hand, up to now, the only NS work where this motion has been quantitatively analyzed, that on BPA-PSF,[36−38] delivers a distribution function of activation energies for the π-flips very similar to that found here for PES (see Figure 12). As we can appreciate in the insert, in addition to the two phenylene rings present in PES, BPA-PSF contains in its monomer the two phenylene rings of the bisphenol-A group. In principle, one could think that the dynamics of these two kinds of rings could be different; for simplicity, in the cited work,[36−38] it was assumed that all rings in BPA-PES behave in the same way. The agreement found here for the distributions of activation energies of both polymers strongly supports the hypothesis made for BPA-PSF rings. Different behaviors for diphenylsulfone and isopropylidene rings would have given rise to at least a much broader distribution function of activation energies in the case of BPA-PSF. Finally, we want to underline another nontrivial result offered by these NS studies: to deliver an independent microscopic confirmation of the geometry of these rotations, supporting the NMR studies.

Concerning the other motion, we can find experimental evidence of oscillations of the phenylene rings in NMR studies on PC[17] and on PEEK.[23] In both works, in addition to the π-flips, oscillations around the same axes are found, of 30° for PC and of "small amplitude" for PEEK. We note that the reported angle for PC oscillations would be very much compatible with our PES results (see insert in Figure 14). Moving to calculations and simulations, such oscillatory motions have also been reported; complete neglect of differential overlap (CNDO) calculations on PC[28] yield "small-amplitude oscillations" together with distributed barrier heights for the π-flips. "Small-angle oscillations" for which amplitudes are also not specified are found from MD-simulations on PC[31] in their 80 ps window. Molecular mechanics calculations on parasubstituted polyaryls (including PES) show that crankshaft rotations introduce "small oscillations" of aromatic rings superimposed on the global rotation of the chain portion.[8] Unfortunately, the information offered in all those works with respect to this motion is very qualitative, preventing a direct comparison with our results. To our knowledge, there is only one work dealing with MD-simulations on PES.[71] Those simulations showed that the paired dihe-

dral angles of successive phenylene rigs in PES change simultaneously following an in-phase rotation. From the trajectories shown at 400 K in that work (up to a maximum time of 30 ps), no evidence for 180° jumps of the rings can be inferred but instead some very rapid motion with a reported average amplitude of about 50°. The average values of the populations of rotational angles obtained by those authors are almost double those deduced in this work for the oscillations (see the insert in Figure 14). On the other hand, the activation energy deduced for the calculated rotational diffusion coefficient D_R (~0.1 eV) is about half of thate found here for the oscillations of the rings. These results prevent the identification of the rotations found by Shi et al. either with the oscillations or with the π-flips of the rings observed by QENS. The results obtained here could be used as a reference for refining the force field used in that work. We may also note that much longer simulation runs are necessary, even at the highest temperature simulated (500 K), to identify and characterize the π-flips by MD-simulations; the time window should reach about the nanosecond scale (see Figure 13). Finally, the comparison of the parameters found for describing PES and BPA-PSF ring oscillations[36,37] are very similar, those determining the distribution function of activation energies (see Figure 12) as well as those concerning the geometry of the motion (see Figure 14). This finding again supports the assumptions made for PES about the dynamical equivalence of the rings. Moreover, the good description obtained for both systems supports the scenario proposed for phenylene rings motion.

We note again the broad character of both processes reflected in the widths of the distribution functions (Figure 12 and, correspondingly, Figure 13). This feature is presumably due to the packing heterogeneity produced by the amorphous character of polymers. The fact that not only the characteristic time of the π-flip process is broadly distributed but also that of the oscillatory motion is noteworthy. A purely intrachain origin of the small amplitude fast motion should in principle lead to a narrow characteristic time distribution.[61] In the scenario proposed, the activation energies in a local environment relate to each other through eq 28. Experimentally, we can thus obtain the ratio $R = \delta E_a^{\pi}/\delta E_a^{\phi}$ that is equivalent to the ratio between the derivatives of the activation energies with respect to the structural parameter ξ,

$$R = \frac{\delta E_a^{\pi}}{\delta E_a^{\phi}} = \frac{\dfrac{dE_a^{\pi}}{d\xi}}{\dfrac{dE_a^{\phi}}{d\xi}} \tag{33}$$

(see also eq 27). The direct mapping of the two distribution functions through eq 28 allows also for the relationship between the activation energies E_a^{π} and E_a^{ϕ} in a local environment, which turns out to be nonlinear. Figure 15 shows the dependence of both magnitudes, E_a^{ϕ} and R, on the activation energy of the π-flip. Since R is higher than 1, E_a^{π} depends in a stronger way on the local packing than does E_a^{ϕ}. The biggest difference between these dependencies occurs for small values of the local potential (presumably for low packing), while for larger potentials (higher packing degree), the oscillatory motion is also clearly affected by packing and R tends to unity. Thus, the broad distribution of characteristic times obtained points to some degree of cooperativity or interchain contribution also for the small-amplitude motion. It is worthy to note at this point the different physical meaning of the activation energies obtained in the proposed framework. Whereas the activation energy for π-flip E_a^{π} represents a real potential barrier over which the phenylene ring jumps, E_a^{ϕ} does not. Oscillations would be caused by rapid fluctuations of the single particle potential; E_a^{ϕ} would then measure the barrier of the molecular motions perturbing the single particle potential for phenylene rings. Therefore, the broadening of the distribution would reflect the correlation between ring oscillations and other molecular motions through fast fluctuations of the local potential. Unfortunately, to our knowledge no data are available in the literature concerning dynamic parameters characterizing the motions of, e.g., the SO_2 group in PES that could be used to check this hypothesis. However, it has to be noticed that, in the case of BPA-PSF, it was possible to relate the activation energy of the ring oscillations with that of the methyl group rotation,[18,72,73] for which time scales are also distributed.[59,60,62,72,73] This suggests some correlation between the two motions, supporting the interpretation proposed for the origin of the oscillations. Finally, regarding the geometry of the oscillatory motion, we comment that a detailed knowledge of the potential landscape could give the key to relate the amplitude of the motion with its activation energy.

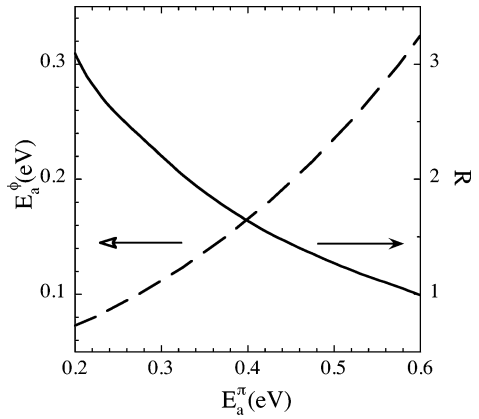

Figure 15. π-flip activation energy dependence of the oscillation energy (dashed line) and the ratio R defined in eq 33 (solid line).

As mentioned in the Introduction, in a large number of studies, the connection of the secondary relaxations in aromatic polymers with phenylene ring motions,[3−6,11,12,15,21,22,24,71] and in particular, of the γ-relaxation with the π-flips, has been invoked.[21,22,24] What about the relation of the reported secondary relaxations in PES and the molecular motions identified here? The observation of a γ-process in PES by means of dynamical mechanical analysis was reported by Aitken et al. in 1992.[4] A transition temperature of 193 K was assigned to this relaxation with measurements at 110 Hz. More recently, a MS study on PES by David et al.[8] reveals three different secondary relaxations denoted by those authors as β_1, β_2, and γ; in adopting the usual nomenclature for the secondary processes, we will refer to those relaxations as γ, β, and δ, respectively. The reported apparent activation energies for those processes are 0.52 eV (γ), 1.04 eV (β), and 0.186 eV (δ). We immediately realize the good agreement between the

apparent activation of the MS γ-relaxation and that of the π-flips on one hand and between the apparent activation energy of the δ-process and that of the oscillations of the phenylene rings on the other hand. In this last case, also, the widths of the distribution functions are very similar [hwhm of about 0.083 eV for the δ-relaxation (see Figure 8 in that work)]. No information was offered for the width of the γ-relaxation. The characteristic times associated with the different processes identified by MS are displayed in Figure 13. As can be seen in this figure, the γ-process shows almost identical relaxation times as those deduced in this work for the phenylene π-flips. The δ-relaxation characteristic times are, however, slower than those observed for the oscillations.

On the other hand, by means of dielectric spectroscopy, Schartel and Wendorff[13] investigated the secondary (γ) relaxation of a set of polyarylates, including PES and the corresponding model systems composed of a single repeat unit and end groups. They found a common activation energy for the γ-relaxation in all systems. The value reported for PES, 0.46 eV, perfectly agrees with that found here for the average activation energy of π-flips. The values of the associated characteristic times [defined as usually as $1/(2\pi\nu_{max})$] are, however, 2 orders of magnitude faster than those obtained for the π-flips, as can be seen in Figure 13.

From the agreements found above for the corresponding activation energies, we can deduce that: (i) the hypothesis of a direct correlation between the γ-relaxation and phenylene π-flips is strongly supported also in PES, and (ii) there is a relation between the δ-process and the oscillations. The discrepancies in the absolute values of the relaxation times might be a consequence of the fact that the relaxations involve not only the respective phenylene motions but also other motions carried out by other components in the polymer. The higher complexity, beyond simple rotations, of the motions behind the secondary relaxations in these kinds of systems has been suggested in a large number of investigations.[1,5,12,21,22,24] Cooperative and interchain packing effects are thought to strongly influence the sub-T_g-observed relaxations.[6,7] Concerning the connection of the oscillations of the phenylene rings with the mechanical δ-relaxation, we may comment that David et al.[8] interpret the widely distributed δ-processes as involving a variety of motions/events, probably local rearrangements of a few rings such as crankshaft-like motions, with possibly a small influence of neighboring chain portions. This is suggested by the low value of the average activation energy of this relaxation and the results of their molecular dynamics calculations. It is important to notice that they explicitly mention the appearance of small oscillations of the aromatic rings introduced by crankshaft rotations. The experimentally observed oscillations might thus be explained in that scenario.

Finally, it is worthy to remark on the importance of identifying the molecular mechanisms taking place in these kinds of systems also for their application as separation membranes. PES is widely used for such purposes. Nowadays, it is believed that gas transport depends on quite a number of ingredients: free volume, chemical affinity between gas and polymer matrix, intermolecular structure, monomeric structure, etc. However, almost nothing is known about the relationship between the polymer structure and mobility at a microscopic level and the parameters characterizing the transport properties as the diffusion coefficient or its associated activation energy. In a recent work,[74] on the basis of results for 46 different glassy polymers with aromatic backbones belonging to four different families (polysulfones, polyarylates, and two kinds of polyimides), a correlation has been found between the gas permeability and the dynamic-mechanical γ-relaxation temperature. This finding, together with the connection established here between π-flips of phenylene rings and the γ-process in PES, implies that such molecular motions might be a key ingredient controlling the gas transport properties in these kinds of systems.

VI. Conclusions

By combining two NS spectrometers covering the microscopic and mesoscopic time scales, we have studied the hydrogen dynamics in glassy PES, revealing the phenylene ring motions.

- At very short times below some picoseconds, a high mobility of the hydrogens is found that might be interpreted in terms of fast librations.
- In addition to π-flips of the aromatic rings, we have observed an additional motion, faster and more restricted in space.
- Because of the structural disorder, both motions show broadly distributed characteristic times, extending over several orders of magnitude.
- The data have been interpreted in terms of a combined motion of the phenylene rings, including π-flips and faster oscillations around the same axis. These last would emerge from the fluctuation of the local phenyl ring environment, and their amplitude increases with temperature.
- The results obtained for the dynamic and geometrical parameters of both motions are very close to those obtained for BPA-PSF.[36,37] This agreement validates the hypothesis made in those works about the dynamical equivalence of isopropylidene and diphenylsulfone rings.
- The coincidence of the activation energies for π-flips and γ-relaxation on one hand and for oscillations and δ-relaxation on the other hand confirms their respective strong correlation. Discrepancies in the absolute values of the corresponding characteristic times reflect the higher complexity of the secondary relaxations.

Acknowledgment. We thank R. Kahn and C. Loirthoir for experimental support at MIBEMOL and D7 instruments, respectively and A. Alegría and S. Arrese-Igor for fruitful discussions and help with the fitting programs. I.Q., A.A., and J.C. acknowledge the University of the Basque Country (Project 9/UPV00206.215-13568/2001) and the Spanish Ministry of Science and Technology (Project MAT 2001/0070) for their support. I.Q. acknowledges a grant from the University of the Basque Country UPV/EHU. Support from "Donostia International Physics Center" is also acknowledged by A.A. and J.C.

References and Notes

(1) Yee, A. F.; Smith, S. A. *Macromolecules* **1981**, *14*, 54.
(2) Fried, J. R.; Letton, A.; Welsh, W. J. In *Order in the Amorphous State of Polymers*; Keinath, S. E., Miller, R. L., Rieke, J. K., Eds.; Plenum: New York and London, 1987.
(3) Fried, J. R.; Letton, A.; Welsh, W. J. *Polymer* **1990**, *31*, 1032.
(4) Aitken, C. L.; McHattie, J. S.; Paul, D. R. *Macromolecules* **1992**, *25*, 2910.

(5) Charati, S. G.; Jog, J. P.; Kulkarni, S. S.; Kulkani, M. G. *J. App. Polym. Sci.* **1994**, *54*, 1093.
(6) Lee, P. L.; Kowalewski, F.; Poliks, M. D.; Shaefer, J. *Macromolecules* **1995**, *28*, 2476.
(7) Plummer, C. J. G.; Soles, D. L.; Xiao, C.; Wu, J.; Kausch, H. H.; Yee, A. F. *Macromolecules* **1995**, *28*, 7157.
(8) David, L.; Girard, C.; Dolmazon, R.; Albrand, M.; Etienne, S. *Macromolecules* **1996**, *29*, 8343.
(9) Xiao, C.; Wu, J.; Yang, L.; Yee, F.; Xie, L.; Gidley, D.; Ngai, K. L.; Rizos, A. K. *Macromolecules* **1999**, *32*, 7913.
(10) Liu, J.; Goetz, J. M.; Schaefer, J.; Yee, A. F.; Li, L. *Macromolecules* **2001**, *34*, 2559.
(11) Katana, G.; Kremer, F.; Fischer, E. W.; Plaetschke, R. *Macromolecules* **1993**, *26*, 3075.
(12) Menegotto, J.; Demont, P.; Bernes, A.; Lacabanne, C. *J. Polym. Sci., Part B: Polym. Phys.* **1994**, *37*, 3494.
(13) Schartel, B.; Wendorff, J. H. *Polymer* **1995**, *36*, 899.
(14) Rizos, A. K.; Petihakis, L.; Ngai, K. L.; Wu, J.; Yee, A. F. *Macromolecules* **1999**, *32*, 7921.
(15) Merenga, A. S.; Papadakis, C. M.; Kremer, F.; Liu, J.; Yee, A. F. *Macromolecules* **2001**, *34*, 76.
(16) Spiess H. W. *Colloid Polym. Sci.* **1983**, *261*, 193.
(17) Schaefer, J.; Stejskal, E. O.; McKay, R. A.; Dixon, W. T. *Macromolecules* **1984**, *17*, 1479.
(18) Schmidt, C.; Kuhn, K. J.; Spiess, H. W. *Colloid Polym. Sci.* **1985**, *71*, 71.
(19) Dumais, J. J.; Cholli, A. L.; Jelinski, L. W.; Hedrick, J. L.; McGrath, J. E. *Macromolecules* **1986**, *19*, 1884.
(20) Roy, A. K.; Jones, A. A.; Inglefield, P. T. *Macromolecules* **1986**, *19*, 1357.
(21) Wehrle, M.; Hellmann, G. P.; Spiess, H. W. *Colloid Polym. Sci.* **1987**, *265*, 265.
(22) Poliks, M. D.; Gullion, T.; Schaefer, J. *Macromolecules* **1990**, *23*, 2678.
(23) Poliks, M. D.; Schaefer, J. *Macromolecules* **1990**, *23*, 3426.
(24) Shi, J. F.; Inglefield, P. T.; Jones, A. A.; Meadows, M. D. *Macromolecules* **1996**, *29*, 605.
(25) Kaji, H.; Tai, T.; Horii, F. *Macromolecules* **2001**, *34*, 6318.
(26) Perchak, D.; Skolnick, J.; Yaris, R. *Macromolecules* **1987**, *20*, 121.
(27) Bicerano, J.; Clark, H. A. *Macromolecules* **1988**, *21*, 585.
(28) Sung, Y. J.; Chen, C. L.; Su, A. C. *Macromolecules* **1990**, *23*, 1941.
(29) Hutnik, M.; Argon, A. S.; Suter, A. W. *Macromolecules* **1991**, *24*, 5970.
(30) Sung, Y. J.; Chen, C. L.; Su, A. C. *Macromolecules* **1991**, *24*, 6123.
(31) Shih, J. H.; Chen, C. L. *Macromolecules* **1995**, *28*, 4509.
(32) Whitney, D. R.; Yaris, R. *Macromolecules* **1997**, *30*, 1741.
(33) Fan, C. F.; Cagin, T.; Shi, W.; Smith, K. A. *Macromol. Theory Simul.* **1997**, *6*, 83.
(34) Tsa, S. F.; Lan, I. K.; Chen, C. L. *Comput. Theor. Polym. Sci.* **1998**, *8*, 283.
(35) Liu, J.; Yee, A. F.; Goetz, J. M.; Schaefer, J. *Macromolecules* **2000**, *33*, 6849.
(36) Arresse-Igor, S.; Arbe, A.; Alegría, A.; Colmenero, J.; Frick, B. *J. Chem. Phys.* **2004**, *120*, 423.
(37) Arresse-Igor, S.; Arbe, A.; Alegría, A.; Colmenero, J.; Frick, B. *J. Chem. Phys.* **2005**, *122*, 049902.
(38) Arresse-Igor, S.; Arbe, A.; Alegría, A.; Colmenero, J.; Frick, B. *Physica B* **2004**, *350*, 211.
(39) Arresse-Igor, S.; Arbe, A.; Alegría, A.; Colmenero, J.; Frick, B. *Appl. Phys. A* **2002**, *74*, S454.
(40) Arresse-Igor, S.; Arbe, A.; Alegría, A.; Colmenero, J.; Frick, B. *Chem. Phys.* **2003**, *292*, 363.
(41) Arresse-Igor, S.; Quintana, I.; Arbe, A.; Colmenero, J.; Alegría, A.; Frick, B.; Janssen, S. *Physica B* **2004**, *350*, e971.
(42) Quintana, I.; A. Arbe, A.; Colmenero, J.; Alegría, A.; Kahn, R. *Physica B* **2004**, *350*, e893.
(43) Springer, T. *Quasielastic Neutron Scattering for the Investigation of Diffusive Motions in Solids, Liquids*; Springer Tracts in Modern Physics; Springer-Verlag: Berlin, Heidelberg, New York, 1972; Vol. 64.
(44) Bée, M. *Quasielastic Neutron Scattering;* Adam Hilger: Bristol, 1988.
(45) Lovesey, S. W. *Theory of Neutron Scattering from Condensed Matter*; Clarendon Press: Oxford, 1984.
(46) Squires, G. L. *Introduction to the Theory of Thermal Neutron Scattering*; Dover Publication: New York, 1996.
(47) The coherent contribution also contains crossed terms involving nuclei of different nature weighed by $b_{coh}{}^{\alpha}b_{coh}{}^{\beta}$, but these can also be neglected for protonated samples.
(48) Alefeld, B.; Birr, M.; Heidemann, A. *Naturwissenschaften* **1969**, *56*, 410.
(49) Frick, B.; Gonzalez, M. *Physica B* **2001**, *201*, 8.
(50) Frick, B.; Richter, D.; Ritter, Cl. *Europhys. Lett.* **1989**, *9*, 557.
(51) Alvarez, F.; Colmenero, J.; Zorn, R.; Willner, L.; Richter, D. *Macromolecules* **2003**, *36*, 238.
(52) See, as recent general references: Andreozzi L., Giordano M., Leporini D., Tosi M., Eds. Special Issue: Third Workshop on Nonequilibrium Phenomena in Supercooled Fluids, Glasses and Amorphous Materials; *J. Phys.: Condens. Matter* **2003**, *15,* nr 11.
(53) See, as recent general references: Ngai, K. L., Floudas, G., Rizos, A. K., Riande, E., Eds. Proceedings of the Fourth International Discussion Meeting on Relaxations in Complex Systems; *J. Non-Cryst. Solids* **2002**, *307*−*310*. Ngai, K. L., Riande, E., Eds. Proceedings of the Third International Discussion Meeting on Relaxations in Complex Systems; *J. Non-Cryst. Solids* **1998**, *235*−*237*. Ngai, K. L., Riande, E., Wright, G. B., Eds. Proceedings of the Second International Discussion Meeting on Relaxations in Complex Systems; *J. Non-Cryst. Solids* **1994**, *172*−*174*. Ngai, K. L., Wright, G. B., Eds. Proceedings of the First International Discussion Meeting on Relaxations in Complex Systems; *J. Non-Cryst. Solids* **1991**, *131*−*133*.
(54) Götze, W. In *Liquids, Freezing, Glass Transition*; Hansen, J. P., Levesque, D., Zinn-Justin, J., Eds.; North-Holland: Amsterdam, 1991; p 287.
(55) Colmenero, J.; Arbe, A. *Phys. Rev. B* **1998**, *57*, 13508.
(56) Colmenero, J.; Arbe, A.; Alegría, A. *Phys. Rev. Lett.* **1993**, *71*, 2603.
(57) Zorn, R.; Arbe, A.; Colmenero, J.; Frick, B.; Richter, D.; Buchenau, U. *Phys. Rev. E* **1995**, *52*, 781.
(58) Arresse-Igor, S. Thesis. University of the Basque Country, 2004.
(59) Chahid, A.; Alegría, A.; Colmenero, J. *Macromolecules* **1994**, *27*, 3282.
(60) Colmenero, J.; Mukhopadhyay, R.; Alegría, A.; Frick, B. *Phys. Rev. Lett.* **1998**, *80*, 2350.
(61) Alvarez, F.; Alegría, A.; Colmenero, J.; Nicholson, T. M.; Davies, G. R. *Macromolecules* **2000**, *33*, 8077.
(62) Moreno, A. J.; Alegría, A.; Colmenero, J.; Frick, B. *Macromolecules* **2001**, *34*, 4886.
(63) Colmenero, J.; Alvarez, F.; Arbe, A. *Phys. Rev. E* **2002**, *65*, 041804.
(64) Howarth, O. W. *J. Chem. Soc., Faraday Trans. 2* **1978**, *74*, 1031.
(65) Howarth, O. W. *J. Chem. Soc., Faraday Trans. 2* **1979**, *75*, 863.
(66) Howarth, O. W. *J. Chem. Soc., Faraday Trans. 2* **1980**, *76*, 1219.
(67) Dejean de la Batie, R.; Lauprêtre, F.; Monnerie, L. *Macromolecules* **1988**, *21*, 2045.
(68) Dejean de la Batie, R.; Lauprêtre, F.; Monnerie, L. *Macromolecules* **1988**, *21*, 2052.
(69) Dejean de la Batie, R.; Lauprêtre, F.; Monnerie, L. *Macromolecules* **1989**, *22*, 122.
(70) Dejean de la Batie, R.; Lauprêtre, F.; Monnerie, L. *Macromolecules* **1989**, *22*, 2617.
(71) Shi, T.; Jiang, W.; An, L.; Li, B. *Macromol. Theory Simul.* **2001**, *10*, 232.
(72) Henrich, P. M.; Nicely, V. A. *Macromolecules* **1991**, *24*, 2506.
(73) Fernandez, D.; Alberdi, J. M.; Colmenero, J. Personal communication.
(74) Singla, S.; Beckham, H. W.; Rezac, M. E. *J. Membr. Sci.* **2002**, *208*, 257.

MA047535N